JMEPEG (2008) 17:785–792
DOI: 10.1007/s11665-008-9233-5


1059-9495/$19.00

# Degradation Characteristics of Elastomeric Gasket Materials in a Simulated PEM Fuel Cell Environment

*Jinzhu Tan, Y.J. Chao, Min Yang, C.T. Williams, and J.W. Van Zee*

*(Submitted April 27, 2007; in revised form December 9, 2007)*

**Polymer electrolyte membrane (PEM) fuel cell stack requires gaskets and seals in each cell to keep the reactant gases (hydrogen and oxygen) within their respective regions. The stability of the gaskets/seals is critical to the operating life as well as the electrochemical performance of the fuel cell. The time-dependant chemical and mechanical degradation of two commercially available silicones-based elastomeric gasket materials in a simulated fuel cell environment was investigated in this work. Two temperatures based on actual fuel cell operation were selected and used in this study. Using optical microscopy, the topographical damage on the sample surface due to the acidic environment was revealed. Atomic adsorption spectrometer analysis shows that silicon, calcium, and magnesium were leached from the materials into the soaking solution. Attenuated total reflection Fourier transform infrared (ATR-FTIR) spectroscopy and X-ray photoelectron spectroscopy (XPS) were employed to study the surface chemistry of the elastomeric gasket materials before and after exposure to the simulated fuel cell environment over time. The ATR-FTIR and XPS test results indicate that the surface chemistry changed significantly and the chemical degradation mechanism is de-crosslinking and chain scission in the backbone. The microindentation test results show that the mechanical properties of the silicone materials changed significantly after exposure to the simulated PEM fuel cell environment over time.**

**Keywords** ATR-FTIR, degradation, elastomeric gasket material, fuel cell, microindentation, XPS

## 1. Introduction

A single proton exchange membrane (PEM) cell consists of end plates, current collectors, flow field channel plates, gaskets, gas diffusion layers, and a membrane electrode assembly (MEA). All these components must be carefully assembled and sealed with gaskets. A typical PEM fuel cell stack used in automotive application may contain over 100 cells. If any gasket degrades or fails during operation or standby, the reactant gases ($O_2$ and $H_2$) can leak overboard or mix each other directly. This will affect the overall operation and performance of the fuel cells, e.g., the cathode cannot be electrically insulated to anode.

Gaskets in PEM fuel cell are typically elastomeric material and are exposed to acidic liquid solution, humid air and hydrogen, as well as subjected to mechanical stress. The long-term stability and durability of the gaskets are critical to both sealing and the electrochemical performance of the fuel cells. In open literatures, there are many reports in which the major emphasis is on both thermal and irradiative degradation on polymeric materials (Ref 1-17). For instance, Youn and Huh (Ref 3) reported the surface degradation of silicone rubber and EPDM under accelerated ultraviolet weathering condition. A severe degradation of the silicone elastomer in a sub-station environment was studied in Ref 17. Chemical degradation of the elastomeric materials was reported in Ref 18-27. A review on the effects and degradation process of silicones in outdoor environment can be found in Graiver et al. (Ref 18). Mitra et al. (Ref 19, 20) investigated the chemical degradation of cross-linked EPDM rubber in 20% $Cr/H_2SO_4$ acidic environment. Time-dependent chemical degradation of a fluoroelastomer in an alkaline environment can be found in Ref 22. Schulze et al. (Ref 23) investigated the degradation of seals in polymer electrolyte fuel cells during fuel cell operation. Although there is a substantial literature discussing chemical degradation of elastomeric gasket materials, few results were reported concerning the degradation and its mechanisms in PEM fuel cell environment.

In this article, the chemical and mechanical degradation of two commercially available elastomeric gasket materials was investigated in a simulated fuel cell environment. The aim of the present study is to study the degree of the degradation and its mechanisms. In an effort toward predicting lifetime, an accelerated durability test (ADT) solution and two temperatures were used in the short-term, accelerated aging tests of the gasket materials. Surface changes were examined using optical microscopy and weight loss was monitored on the samples exposed to the simulated fuel cell environment at selected exposure time. The chemical degradation on the surface of the gasket materials after exposure to the simulated fuel cell environment over time was studied using ATR-FTIR spectroscopy and XPS. Atomic adsorption spectrometry was used to

**Jinzhu Tan**, College of Mechanical and Power Engineering, Nanjing University of Technology, Nanjing, Jiangsu 210009, China; **Jinzhu Tan, Y.J. Chao,** and **Min Yang**, Department of Mechanical Engineering, University of South Carolina, 300 S. Main, Columbia, SC 29208; **Min Yang**, School of Materials Science and Engineering, Shandong University, Jinan, Sandong 250061, China; and **C.T. Williams** and **J.W. Van Zee**, Department of Chemical Engineering, University of South Carolina, 300 S. Main, Columbia, SC 29208. Contact e-mail: chao@sc.edu.

identify the chemicals leached from the gasket samples into the soaking solution. The microindentation test method was used to assess the change of mechanical properties of the materials before and after exposure to the environment.

## 2. Experiments

### 2.1 Materials and Simulated Fuel Cell Environment

Two commercial elastomeric sealing materials, silicone S and silicone G, were used in this study. The silicone S rubber is a two-part formulation liquid injection molded material. It mainly contains polydimethylsilicoxane with vinyl functionalities in part A and polydimethylsilicoxane with hydrosilylation functionalities in part B. Parts A and B (1:1) were combined and heated to crosslink under the platinum catalyzed reaction. The crosslinking reaction mechanism is hydrosilylation. The chemistry for the silicone G rubber is similar to that for silicone S. Silicone materials are chosen because of their wide temperature operating range, low cost, and ease of fabrication, and are widely used as sealing materials, including in fuel cells (Ref 23, 28).

An accelerated durability test (ADT) solution for short-term accelerated aging tests was used as the simulated fuel cell environment for this study. Forty-eight percent HF and ninety-eight percent $H_2SO_4$ were dissolved in balance reagent grade water to make the ADT solution. The composition of the ADT solution is 1 M $H_2SO_4$, 10 ppm HF and reagent grade water having 18 MΩ resistance as the exposure medium.

The test temperatures were 80 and 60 °C, which are close to the operating temperatures of actual PEM fuel cells.

### 2.2 Aging and Characterization Methods

Rectangular-shaped specimens were prepared and exposed to the ADT solution. The dimensions of the silicone S specimen are 40 mm in length, 10 mm in width, and 1.0 mm in thickness. The dimensions for the silicone G specimen are 40 mm in length, 10 mm in width, and 3.2 mm in thickness. The tests were performed at temperatures of 80 and 60 °C and exposed to ADT solutions from 1 to 45 weeks. The change in weight over time was monitored on the samples. The surface conditions of the samples were examined before and after exposure to the solutions using optical microscope (Leco, OLYMPUS PME-3) at selected times.

The samples were submerged in the ADT solution bottles at 80 and 60 °C. The aged samples were taken out of the test bottle at selected times. The ATR-FTIR spectroscopy was performed on the surface of the gasket samples using a Nexus Model 670 Instrument (Nicolet Instrument Corporation) and run with 128 scans at a resolution of 4 $cm^{-1}$. The infrared radiation (IR) penetrates the surface of the test sample to approximately 1 μm.

Samples with 15 mm in length, 10 mm in width, and 1-3.2 mm in thickness were prepared and exposed to ADT solution at 80 and 60 °C. The aged samples were taken out of the test bottles at selected times for XPS analysis using a Kratos AXIS 165 spectrometer with monochromatic Al $K_\alpha$ (1486.71 eV) X-ray source operated at a take-off angle of 90° in a probe depth of 3-5 nm. The pressure used in the XPS chamber was about $2.67 \times 10^{-7}$ Pa and increased to approximately $2.53 \times 10^{-5}$ Pa during ion bombardment. The survey spectra in the range of 0-1200 eV were recorded in 1 eV step for each sample. Atomic concentrations of each element were calculated by determining the relevant integral peak intensities. High-resolution analysis was performed in the carbon 1s ($C_{1s}$) and the silicon 2p ($Si_{2p}$) regions. The spectra were deconvoluted by curve fitting. The high-resolution spectra were recorded in 0.1 eV steps from which the detailed compositions were calculated. The full width at half maximum (FWHM) for all peaks were constrained to 1-2.0 eV.

Note that in order to avoid the effect of the remaining ADT solution on the sample surface on the ATR-FTIR and XPS results, the surface of the samples was cleaned using reagent grade water having 18 MΩ resistance to remove the excess of free acids and made dry at room temperature before the ATR-FTIR and XPS analysis.

In order to assess the mechanical properties of the samples after exposure to the simulated PEM fuel cell environment, microindentation tests were performed on the samples after exposure of 45 weeks. The microindenter (CETR, Campbell CA) monitors and records the load and displacement of the indenter. The tip of the indenter is a stainless steel ball with a radius of 1.98 mm. The instrument has a force resolution of 0.5 mN and a displacement resolution of 0.1 μm. In all the analysis, the materials without exposure to the ADT solution were also characterized for comparison.

In addition, the solution exposed to each sample was taken out at selected time and analyzed for leachants using atomic adsorption spectrometry (Perkin Elmer 3300).

## 3. Results and Discussion

### 3.1 Microscopy

Optical microscopy was used to visually observe the degradation of the surface of the material in our study. Figures 1 and 2 show the optical micrographs for silicone S, silicone G, respectively, before and after exposure to ADT solution at 80 and 60 °C at selected times. The magnification used was 500×.

For the silicone S samples, the optical micrographs in Fig. 1 clearly show that surface conditions were changed over time from initially smooth to rough, cracked surface and finally crack propagation. Small cracks appeared on the surface at 80 °C after 3 weeks exposure to ADT solution (see Fig. 1). The crack size increased with exposure time after that, and eventually the sample became colored on the surface and broke after 45 weeks. The extent of surface damage at 80 °C is more severe compared to 60 °C under identical conditions (see Fig. 1d-h).

Figure 2 shows optical micrographs of silicone G samples before and after 17 weeks exposure to ADT solution. It can be seen that the surface conditions of the samples were changed over time from initially smooth to rough (see Fig. 2b and c), but no cracks up to 45 weeks. Relatively, silicone G sample is more stable than silicone S sample under the same test environment.

It can be concluded that (a) the surface topography of the two materials exhibits time-dependent chemical degradation, (b) temperature has a significant effect, and (c) silicone S degraded more severely for the two materials.

### 3.2 Weight Loss

The samples were taken out from the test chamber at selected times. The surface of the sample was cleaned using

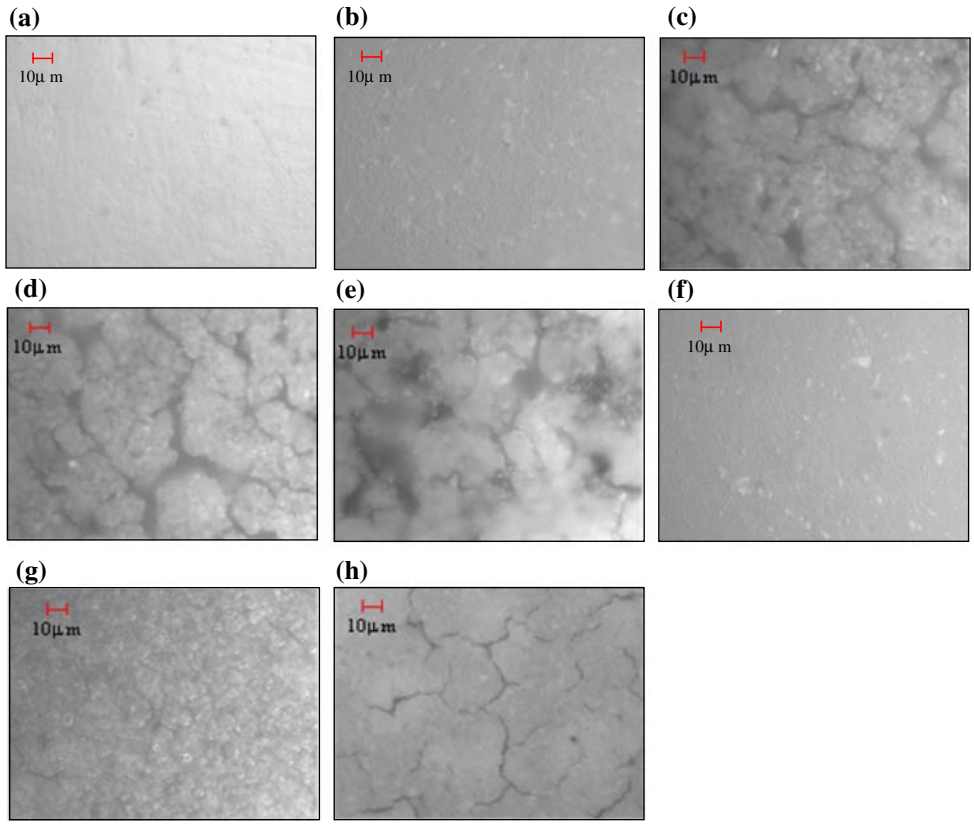


**Fig. 1** Optical micrographs of silicone S samples before and after exposure to ADT solution at 80 and 60 °C at various exposure times. (a) Before exposure, (b) 1-week exposure at 80 °C, (c) 3-week exposure at 80 °C, (d) 5-week exposure at 80 °C, (e) 17-week exposure at 80 °C, (f) 5-week exposure at 60 °C, (g) 17-week exposure at 60 °C, and (h) 45-week exposure at 60 °C

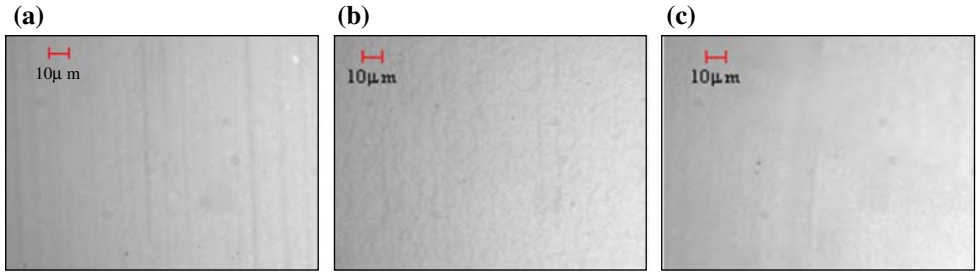


**Fig. 2** Optical micrographs of silicone G samples before and after exposure to ADT solution at 80 and 60 °C at various exposure times. (a) Before exposure, (b) 17-week exposure at 80 °C, and (c) 17-week exposure at 60 °C

reagent grade water having 18 MΩ resistance to remove the excess acids and made dry at room temperature before the weight change was monitored. Figure 3 shows the change of weight from the samples in the ADT solution at 80 and 60 °C. In the figure, silicone S and silicone G are represented by SS and SG, respectively. It is shown that silicone S is the most affected. The weight loss was about 58.5% (not shown in Fig. 3) for silicone S after 45 weeks in the ADT solution at 80 °C. About 14.7% (not shown in Fig. 3) was found after exposure of 45 weeks in the ADT solution at 60 °C. The weight lost for silicone G was 6.0 and 2.4% (not shown in Fig. 3) after 45 weeks in the ADT solution at 80 and 60 °C, respectively. The results from weight loss in this current study is similar to those in our previous work (Ref 26, 27) in which samples having 90 and 120° bend angles were investigated.

It can be concluded from this study that (a) temperature has a significant effect on the weight loss and (b) comparatively silicone S had the more weight loss.

### 3.3 ATR-FTIR

The aim of the ATR-FTIR analysis is to determine the chemistry changes as an indication of chemical degradation that occurred to the elastomeric gasket materials in the simulated PEM fuel cell environment. The spectra for the two materials before and after various exposure times to the simulated fuel cell environment are shown in Fig. 4-6.

**3.3.1 Silicone S.** Figure 4 shows the results of ATR-FTIR for the silicone S sample before exposure (a) and after 17 week (b) exposure to ADT solution at 80 °C. Figure 5 shows the

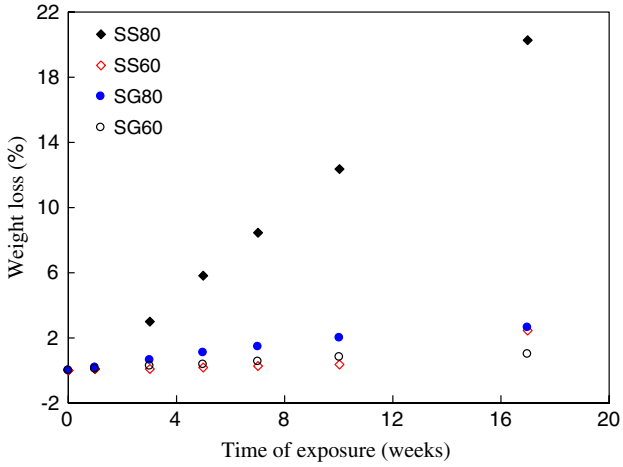


**Fig. 3** Weight change with exposure time for the samples

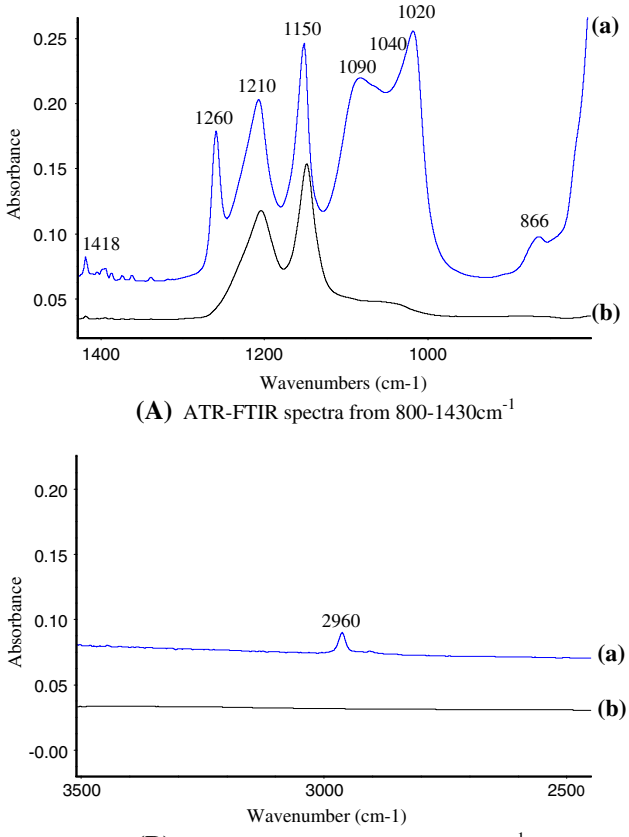


**Fig. 4** Comparison of ATR-FTIR spectra for silicone S in ADT solution at 80 °C: (a) without exposure and after (b) 17 weeks exposure

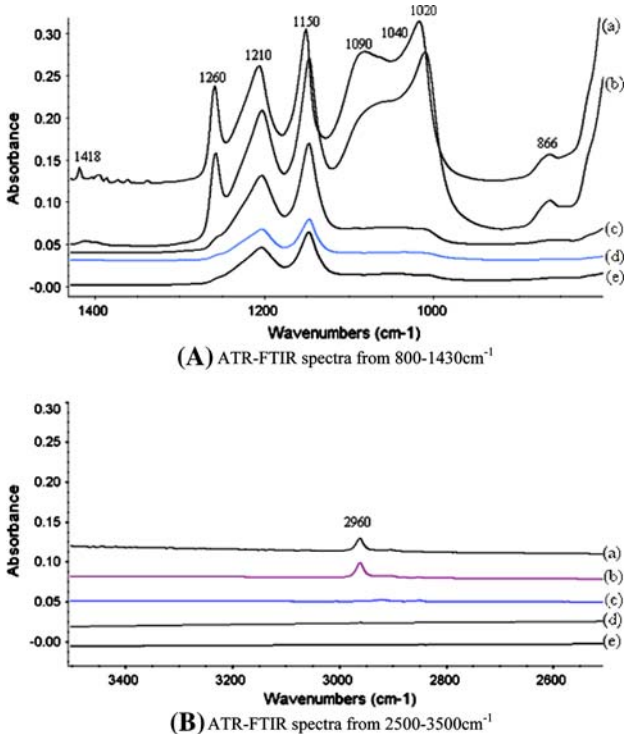


**Fig. 5** Comparison of ATR-FTIR spectra for silicone S in ADT solution at 60 °C: (a) without exposure and after (b) 1 week, (c) 3 weeks, (d) 5 weeks, and (e) 7 weeks exposure

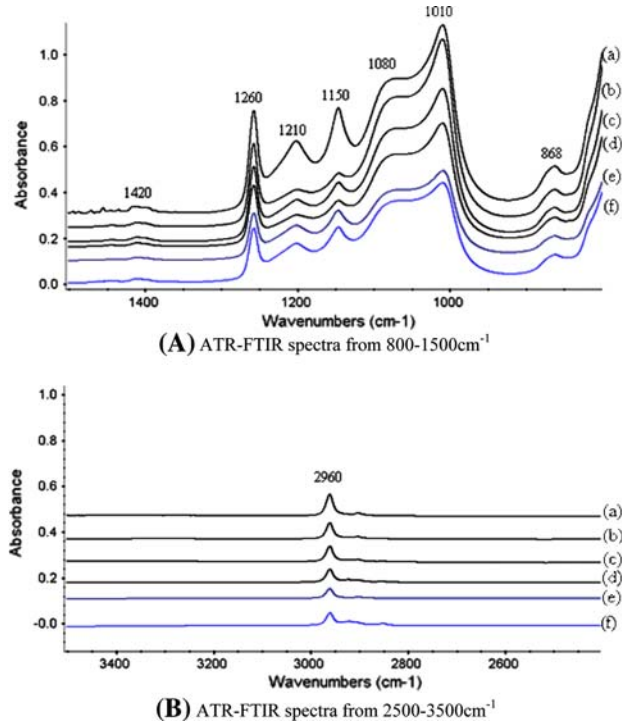


**Fig. 6** Comparison of ATR-FTIR spectra for silicone G in ADT solution at 80 °C: (a) without exposure and after (b) 1 week, (c) 3 weeks, (d) 5 weeks, (e) 7 weeks, and (f) 10 weeks exposure

results of the ATR-FTIR analysis for silicone S sample before exposure (a) and after 1 week (b), 3 week (c), 5 week (d), and 7 week (e) exposure to the ADT solution at 60 °C. As expected, both spectra of the unexposed virgin samples [see Fig. 4A(a) and 5A(a)] are the same. The strongest and broadest peaks for the unexposed samples [shown in Fig. 4A(a) and 5A(a)] are between 1020 and 1090 $cm^{-1}$ which are from the stretching vibrations of Si-O-Si present in the silicone S backbone. The correspondence between the spectrum and the vibration mode, here and throughout the rest of the article, was obtained from the handbook (Ref 29). It can also be seen that

the long chain siloxanes have two broad IR peaks near 1020 and 1090 $cm^{-1}$. The peaks at 1260 and 866 $cm^{-1}$ are from the bending vibration of Si-$CH_3$ and the rocking vibration of Si-$CH_3$. The peaks at 2960 $cm^{-1}$ (shown in Fig. 4B and 5B) are from the stretching vibration mode of $CH_3$. The peaks near 1418 $cm^{-1}$ (Fig. 4A and 5A) are from the rocking vibration of –$CH_2$– as a part of the silicone S crosslinked domain.

Test results in our previous work (Ref 27) showed that the intensities of the peaks at 1020 and 1090, 866, 1260, 1418, and 2960 $cm^{-1}$ decreased sharply after 1 week exposure and then almost disappeared after 3-week exposure at 80 °C. In the present work, these peaks disappeared almost completely after 17-week exposure. A group of new peak apparently appeared at the spectrum near 1040 $cm^{-1}$ due to the formation of Si-O as a consequence of chemical changes (see Fig. 4). Furthermore, the intensity of the new peak increased with the exposure time indicating continued evolution of the material.

The trends observed at 60 °C (Fig. 5) are similar to those in 80 °C (Fig. 4) that some peak intensities decreased and some others emerged after exposure to the solutions. The intensities at 1020 and 1090, 866, 1260, 1418, and 2960 $cm^{-1}$ decreased sharply after 3 weeks and then almost disappeared after 5 weeks as shown in Fig. 5. A new peak was emerged at the spectrum near 1040 $cm^{-1}$, which is likely due to stretching vibration of Si-O as the chemistry changes. Its intensity increased with the exposed time up to 45 weeks at 60 °C (not shown in Fig. 5).

It is concluded that there are significant chemical changes in both rubber backbone and the crosslinked domain for silicone S samples exposed to ADT solution at 80 and 60 °C over time. It is believed that the chemical degradation is likely due to de-crosslinking and chain scissoring in the rubber backbone for the environment.

**3.3.2 Silicone G.** The results from the ATR-FTIR analysis for silicone G samples before and after exposure to ADT solution at 80 °C at various times are shown in Fig. 6. The ATR-FTIR spectrum for unexposed silicone G sample is shown in Fig. 6A(a), which is nearly identical to those shown in Fig. 4A(a) and 5A(a) for silicone S. The strongest and broadest peaks for the unexposed data [in Fig. 6A(a)] are between 1010 and 1080 $cm^{-1}$ due to the stretching vibrations of Si-O-Si in the backbone. It can also be seen that the long chain siloxanes have two broad IR peaks near 1010 and 1080 $cm^{-1}$. The peaks at 1260 and 868 $cm^{-1}$ are from the bending vibration of Si-$CH_3$ and the rocking vibration of Si-$CH_3$, respectively. The peak at 2960 $cm^{-1}$ (shown in Fig. 6B) is from the stretching vibrations of $CH_3$. The peak around 1420 $cm^{-1}$ is from the rocking vibration of –$CH_2$– present as a part of the silicone G crosslinked domain. In Fig. 6, the intensity of the peaks between 1010 and 1080 $cm^{-1}$ decreased slightly with exposure time at 80 °C (see Fig. 6A). The peaks at 868, 1260, and 1420 $cm^{-1}$ in Fig. 6A and 2960 $cm^{-1}$ in Fig. 6B also showed similar trend. Similar observations are made for silicone G samples exposure to ADT solution at 60 °C, although the extent of decrease of the intensity at 2960, 868, 1260, 1420, 1010, and 1080 $cm^{-1}$ at 60 °C is slightly lower than that at 80 °C under identical conditions.

Compared to silicone S, the degradation mechanisms for silicone G are similar except that the extent of degradation for silicone S is more severe than that for silicone G. It may be concluded that silicone G is more stable chemically than silicone S under the test conditions.

### 3.4 X-ray Photoelectron Spectroscopy

Figure 7 shows XPS survey spectra for silicone G samples before and after 4-week exposure to ADT solution at 80 °C. The spectra revealed the presence of carbon (C), oxygen (O), silicon (Si), and fluorine (F). The presence of F in Fig. 7B may result from the environment occurred on the surface of sample. The atomic concentration of these elements for the silicone G sample are given in Table 1. Table 1 shows the ratios of concentration (C/Si and O/Si) before and after exposure time. The XPS results for silicone S sample in our previous work (Ref 27) are also listed in Table 1 for comparison. It can be seen from Table 1 that the C/Si ratio decreased and the O/Si ratio increased slightly with increasing exposure time for the silicone G sample. The decrease of C/Si ratio and increase of O/Si ratio with exposure time could be due to that the methyl group on the silicon atom was attached and the chain in the backbone was broken. The change of chemical components reflects the chemical degradation of the materials exposed to the environment.

It can be seen from Table 1 that the trends in silicone G are similar to those in silicone S. The decrease of C/Si ratio and increase of O/Si ratio for silicone G are less under identical conditions, e.g., the amount of the decrease of C/Si ratio is 0.38 for silicone G after 4-week exposure, whereas it is 1.60 for silicone S under the same test conditions. The results indicate that silicone G is more stable chemically than silicone S. The XPS results are in agreement with the FTIR observations.

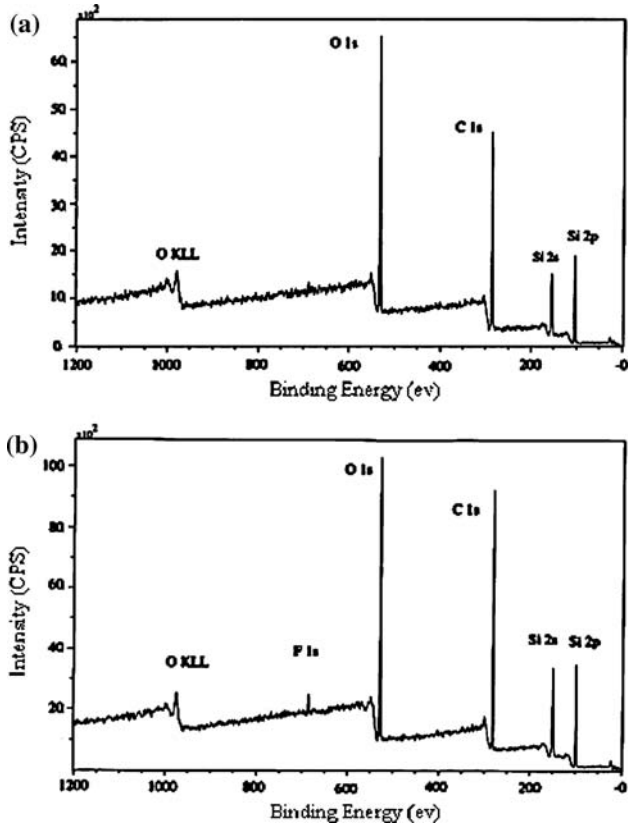


**Fig. 7** XPS spectra for silicone G (a) sample before and (b) after 4 week exposure to ADT solution at 80 °C

**Table 1 Surface atomic concentration of each element and radios of atomic concentrations of O and C to Si**

| Sample | Exposure time | Atomic concentration, at.% | | | | Ratios to Si | |
|---|---|---|---|---|---|---|---|
| | | C | O | Si | F | C/Si | O/Si |
| Silicone G | Before exposure | 53.29 | 26.0 | 20.71 | 0.0 | 2.57 | 1.26 |
| | 1 week exposure | 48.69 | 29.22 | 21.51 | 0.58 | 2.26 | 1.36 |
| | 4 week exposure | 48.38 | 28.87 | 22.03 | 0.72 | 2.19 | 1.31 |
| Silicone S [27] | Before exposure | 51.36 | 27.56 | 20.41 | 0.67 | 2.52 | 1.35 |
| | 1 week exposure | 32.82 | 38.10 | 23.03 | 6.05 | 1.43 | 1.65 |
| | 4 week exposure | 23.13 | 51.81 | 25.06 | 0.0 | 0.92 | 2.07 |

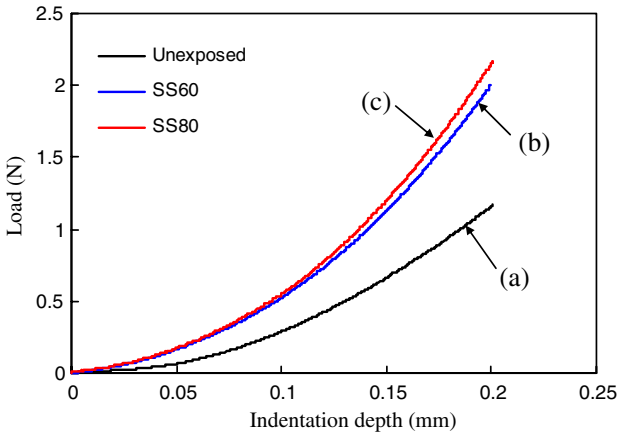


**Fig. 8** Load-indentation depth curves of silicone S samples before exposure (a) and after 45-week exposure to ADT solution at 60 °C (b) and 80 °C (c)

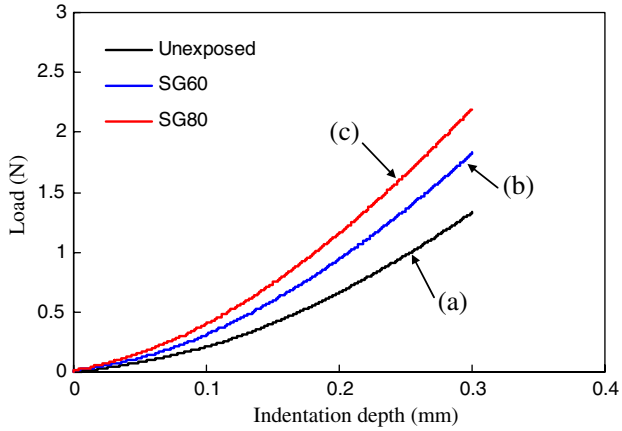


**Fig. 9** Load-indentation depth curves of silicone G samples before exposure (a) and after 45-week exposure to ADT solution at 60 °C (b) and 80 °C (c)

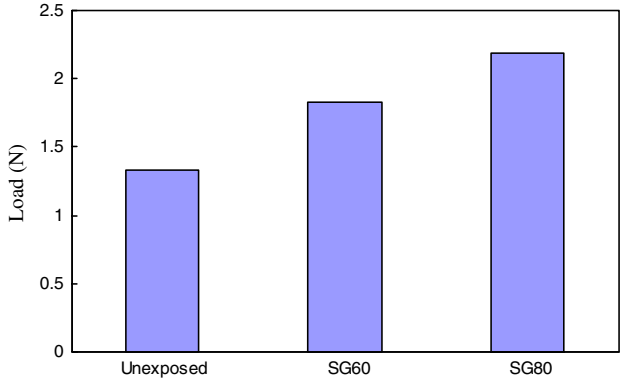


**Fig. 10** Bar charts of indentation load for silicone G samples before exposure (unexposed) and after 45-week exposure to ADT solution at 60 °C (SG60) and 80 °C (SG80) at a peak penetration depth of 0.30 mm

### 3.5 Microindentation Test Results

**3.5.1 Indentation Load.** Figure 8 shows the indentation load-depth curves for the unexposed silicone S sample (Fig. 8a) and the samples after 45-week exposure at 60 °C (Fig. 8b) and 80 °C (Fig. 8c). Figure 9 shows the indentation load-depth curves for the unexposed silicone G sample (Fig. 9a) and the samples after 45-week exposure at 60 °C (Fig. 9b) and 80 °C (Fig. 9c). Displacement controlled test was used in this test at a peak indentation depth of 0.20 and 0.30 mm for silicone S and silicone G, respectively. Here, we use the indentation load at the peak indentation depth as a manifestation of the surface hardening of the samples. Figure 10 shows bar charts of indentation load for the silicone G samples before exposure (unexposed), and after 45-week exposure at 60 °C (SG60) and 80 °C (SG80) at a peak indentation depth of 0.30 mm. In Fig. 8-10, SS80, SS60, SG80, and SG60 represent the exposed samples at 80 and 60 °C for silicone S and silicone G, respectively. From Fig. 8-10, the sample exposed to the ADT solution at 80 °C has the largest indentation load, followed by the sample at 60 °C and then the virgin sample. The results indicate that the samples exposed to the environment hardened over time. The extent of the surface hardening at 80 °C is more than that at 60 °C.

**3.5.2 Hertz Contact Modeling.** Hertz contact theory was often used to obtain the elastic modulus from the indentation load-indentation depth curves (Ref 30, 31). Based on the Hertz theory of elastic contact, considering the contact between a rigid sphere (the indenter tip) and a flat surface (the silicone rubber sample), the relationship between the total displacement of both the indenter and sample, δ, and the load $P$ can be written as (Ref 30)

$$\delta = \left(\frac{9P^2}{16RE^{*2}}\right)^{1/3} \quad \text{(Eq 1)}$$

where $R$ is the radius of indenter, $E^*$ is a combination of the modulus of the indenter and the sample and can be given by

$$\frac{1}{E^*} = \frac{1-\nu_{\text{indenter}}^2}{E_{\text{indenter}}} + \frac{1-\nu_{\text{sample}}^2}{E_{\text{sample}}} \quad \text{(Eq 2)}$$

where $E_{\text{indenter}}$ and $E_{\text{sample}}$ are the elastic modulus and $\nu_{\text{indenter}}$ and $\nu_{\text{sample}}$ are the Poisson's ratios of the indenter and the sample, respectively. Equation 1 can be rewritten as

$$E^* = \frac{3}{4\sqrt{R}} P\delta^{-1.5} \quad \text{(Eq 3)}$$

When a rigid indenter compresses a soft flat sample like the silicone rubber samples used in this study, δ is the depth of the

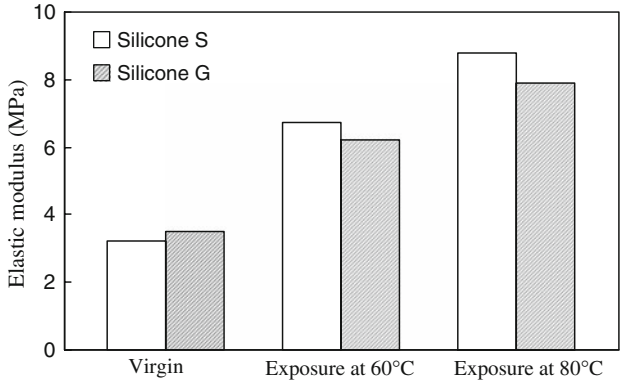


**Fig. 11** Elastic modulus for silicone S and silicone G samples before exposure (Virgin) and after 45-week exposure to ADT solution at 60 and 80 °C

indentation because the steel indenter's deformation is negligible relative to that of the rubber sample. Based on Eq 3 and experimental indentation load and indentation depth, the elastic modulus of the sample can be obtained. The elastic modulus and Poisson's ratio of the stainless steel indenter tip were assumed as $2.0 \times 10^{11}$ Pa and 0.3, respectively (Ref 31). The Poisson's ratio for the silicone rubber sample was assumed as 0.49 (Ref 32). Combining Eq 2 and 3, the elastic moduli for the two materials were calculated and are shown in Fig. 11. It can be seen from Fig. 11 that the silicone S samples exposed to the ADT solution at 80 °C show the highest elastic modulus, followed by the sample at 60 °C and then the unexposed sample. The tread is similar for silicone G samples. The result is in agreement with the indentation load result as shown in Fig. 10. These results indicate that the elastic modulus changed significantly due to the chemical degradation after exposure to the solution.

Compared to silicone G, the degradation for silicone S is similar (see Fig. 11); however, the extent of degradation for silicone S is more severe than that for silicone G. The results are in agreement with the FTIR and XPS observations.

### 3.6 Atomic Adsorption Spectrometry

In order to identify the foreign materials leached from the gasket samples into the soaking solution, the atomic adsorption spectrometry was employed to analyze the solution. Silicon, calcium, and magnesium were identified in the solution. Table 2 shows the silicon, calcium, and magnesium values for the samples after 45-week exposure to ADT solution at 80 and 60 °C. Data in Table 2 show that the silicon ions in solution had the highest concentration under identical test conditions.

It is noted that fillers in elastomeric compounds are required to enhance the mechanical properties, e.g., tensile strength, hardness, resistance to compression set, for gasket or sealing applications. Our study indicates that when the gasket samples were submerged in the simulated PEM fuel cell solution, some of the fillers such as silicon dioxide, magnesium oxide, and calcium carbonate were attacked by the solution. Consequently, silicon, calcium, and magnesium were formed and detected in the soaking solution. These chemicals may be detrimental to the electro-chemical process of PEM fuel cells.

**Table 2 Values of silicon, calcium, and magnesium (mg/L)**

| Sample | Exposure time (weeks) | 80 °C | | | 60 °C | | |
|---|---|---|---|---|---|---|---|
| | | Si | Ca | Mg | Si | Ca | Mg |
| Silicone S | 45 | 282.66 | 40.70 | 1.93 | 254.67 | 26.07 | 1.17 |
| Silicone G | 45 | 176.77 | 0.26 | 0.07 | 88.74 | 0.11 | 0.04 |

## 4. Conclusion

Chemical and mechanical degradation of two available commercial elastomeric gasket materials was studied in simulated fuel cell environment in this work. The following conclusion can be made.

1. The two materials degraded upon exposure to the simulated EPM fuel cell environment. Temperature has a significant effect to the degradation. The higher the temperature, the faster the material degraded. Relatively, silicone S is more affected by temperature.
2. Optical microscopy shows that the degradation started from surface roughness and finally resulted in cracks on the surface after exposure to the environment over time.
3. ATR-FTIR and XPS results reveal that the surface chemistry changed significantly, indicating a chemical degradation of the two materials. The degradation mechanisms of silicone S proceeded via de-crosslinking and chain scissoring in the rubber backbone. The degradation mechanism of silicone G is similar, but with less degree. The results indicate that silicone G is more stable than silicone S under the same test conditions.
4. The microindentation test results show that the mechanical properties of the two materials changed significantly after exposure to the simulated PEM fuel cell environment over time. The extent of degradation for silicone S is more severe than that for silicone G.
5. Atomic adsorption spectrometry detected silicon, calcium, and magnesium leached from the gasket materials into the soaking solution. Among them, the silicon ions in solution showed the highest concentration under identical conditions.
6. Based on the present results, it may be concluded that the silicone G material is a better choice than the silicone S material for PEM fuel cell applications.

## Acknowledgments

The work was sponsored by the NSF Industry/University Cooperative Research Center for Fuel Cells at the University of South Carolina. Encouragement from the industry partners and financial support from the center were greatly appreciated. The assistance from Drs. Xiaodong Li, Xinnan Wang, Woo-Kum Lee, and C. C. Stork is acknowledged.

## References

1. S. Kole, K. Srivastava, D.K. Tripathy, and A.K. Bhowmick, Accelerated Hydrothermal Weathering of Silicone Rubber, *J. Appl. Polym. Sci.*, 1994, **54**(9), p 1329–1337

2. A.K. Bhowmick, J. Konar, S. Kole, and S. Narayanan, Surface Properties of EPDM, Silicone Rubber, and Their Blend During Aging, *J. Appl. Polym. Sci.*, 1995, **57**(5), p 631–637
3. B.H. Youn and C.S. Huh, Surface Degradation of HTV Silicone Rubber and EPDM Used for Outdoor Insulators Under Accelerated Ultraviolet Weathering Condition, *IEEE Trans. Dielect. Electr. Insul.*, 2005, **12**(5), p 1015–1024
4. J. Konar, G. Samanta, B.N. Avasthi, and A.K. Sen, Oxidative Degradation of EPDM Rubber Using Phase Transferred Permanganate as Oxidant, *Polym. Degrad. Stab.*, 1994, **43**(2), p 209–216
5. T. Zaharescu and M. Giurginca, *Proceedings of the 1995 IEEE 5th International Conference on Conduction and Breakdown in Solid Dielectric*. Leicester, England, 1995, p 472–476
6. T. Zaharescu, M. Giurginca, and S. Jipa, Radiochemical Oxidation of Ethylene-Propylene Elastomers in the Presence of Some Phenolic Antioxidants, *Polym. Degrad. Stab.*, 1999, **63**(2), p 245–251
7. R.A. Assink, M. Celina, K.T. Gillen, R.L. Clough, and T.M. Alam, Morphology Changes During Radiation-Thermal Degradation of Polyethylene and an EPDM Copolymer by $^{13}C$ NMR Spectroscopy, *Polym. Degrad. Stab.*, 2001, **73**(2), p 355–362
8. T. Zaharescu, E. Feraru, and C. Podina, Thermal Stability of Gamma Irradiated Ethylene-Propylene-Diene Monomer/Divinyl Benzene Systems, *Polym. Degrad. Stab.*, 2005, **87**(1), p 11–16
9. A. Ghanbari-Siahkali, S. Mitra, P. Kingshott, K. Almdal, C. Bloch, and H.K. Rehmeier, Investigation of the Hydrothermal Stability of Crosslinked Liquid Silicone Rubber (LSR), *Polym. Degrad. Stab.*, 2005, **90**(3), p 471–480
10. A.N. Chaudhry and N.C. Billingham, Characterization and Oxidative Degradation of a Room-temperature Vulcanized Poly(dimethylsiloxane) Rubber, *Polym. Degrad. Stab.*, 2001, **73**(3), p 505–510
11. M.A. Kader and A.K. Bhowmick, Thermal Ageing, Degradation and Swelling of Acrylate Rubber, Fluororubber and Their Blends Containing Polyfunctional Acrylates, *Polym. Degrad. Stab.*, 2003, **79**(2), p 283–295
12. M. Patel, A.R. Skinner, and R.S. Maxwell, Sensitivity of Condensation Cured Polysiloxane Rubbers to Sealed and Open-to Air Thermal Ageing Regimes, *Polym. Test.*, 2005, **24**(5), p 663–668
13. L. Zhang, Z. Xu, Q. Wei, and S. He, Effect of 200 keV Proton Irradiation on the Properties of Methyl Silicone Rubber, *Radiat. Phys. Chem.*, 2006, **75**(2), p 350–355
14. R.L. Hauser, R. Hauser Quick Jr, Allen N, Williams AE, Sulfurous Vapors Emitted from EPDM Rubber can Damage Electronic Instruments, *Rubber World*, 2001, **224**(5), p 24–26
15. A.U. Paeglis, A Simple Model for Predicting Heat Aging of EPDM Rubber, *Rubber Chem. Technol.*, 2004, **77**(2), p 242–256
16. M. Ehsani, H. Borsi, E. Gockenbach, G.R. Bakhshandeh, and J. Morshedian, Modified Silicone Rubber for Use as High Voltage Outdoor Insulators, *Adv. Polym. Technol.*, 2005, **24**(1), p 51–56
17. H. Liu, G. Cash, D. Birtwhistle, and G. George, Characterization of a Severely Degraded Silicone Elastomer HV Insulator – An Aid to Development of Lifetime Assessment Techniques, *IEEE Trans. Dielect. Electr. Insul.*, 2005, **2**(3), p 478–486
18. D. Graiver, K.W. Farminer, and R. Narayan, A Review of the Fate and Effects of Silicones in the Environment, *J. Polym. Environ.*, 2003, **11**(4), p 129–136
19. S. Mitra, A. Ghanbari-Siahkali, P. Kingshott, H.K. Rehmeier, H. Abildgaard, and K. Almdal, Chemical Degradation of Crosslinked Ethylene-Propylene-Diene Rubber in an Acidic Environment, Part I: Effect on Accelerated Sulphur Crosslinks, *Polym. Degrad. Stab.*, 2006, **91**(1), p 69–80
20. S. Mitra, A. Ghanbari-Siahkali, P. Kingshott, H.K. Rehmeier, H. Abildgaard, and K. Almdal, Chemical Degradation of Crosslinked Ethylene-Propylene-Diene Rubber in an Acidic Environment, Part II: Effect of Peroxide Crosslinking in the Presence of a Coagent, *Polym. Degrad. Stab.*, 2006, **91**, p 81–93
21. T. Sugama, Surface Analysis of Fluoroelastomer Bearigs Exposed to Geothermal Environments, *Mater. Lett.*, 2001, **50**(2–3), p 66–72
22. S. Mitra, A. Ghanbari-Siahkali, P. Kingshott, K. Almda, H.K. Rehmeier, and A.G. Christensen, Chemical Degradation of Fluoroelastomer in an Alkaline Environment, *Polym. Degrad. Stab.*, 2004, **83**, p 195–206
23. M. Schulze, T. Knori, A. Schneider, and E. Gulzow, Degradation of Sealings for PEFC Test Cells During Fuel Cell Operation, *J. Power Sources*, 2004, **127**(1–2), p 222–229
24. B. Marungsri, H. Shinokubo, R. Matsuoka, and S. Kumagai, Effect of Specimen Configuration on Deterioration of Silicone Rubber for Polymer Insulators in Salt Fog Ageing Test, *IEEE Trans. Dielect. Electr. Insul.*, 2006, **13**(1), p 129–138
25. D.E. Curtin, R.D. Lousenberg, T.J. Henry, P.C. Tangeman, and M.E. Tisack, Advanced Materials for Improved PEMFC Performance and Life, *J. Power Sources*, 2004, **131**, p 41–48
26. J. Tan, Y.J. Chao, W.K. Lee, C.S. Smith, J.W. VanZee, and C.T. Williams, *Proceedings of the 4th International Conference on Fuel Cell Science, Engineering and Technology.* Irvine, CA, 2006
27. J. Tan, Y.J. Chao, J.W. VanZee, and W.K. Lee, Degradation of Elastomeric Gasket Materials in PEM Fuel Cells, *Mater. Sci. Eng. A*, 2007, **445–446**, p 669–675
28. D. A. Dillard, S. Gao, M.W. Ellis, J.J. Lesko, J.G. Dillard, and J. Sayre, B. Vijayendran, *Second International Conference on Fuel Cell Science, Engineering and Technology.* Rochester, NY, 2004, p 553–560
29. D. Lin-Vien, N.B. Colthup, W.G. Fateley, and J.G. Grasselli, *The Handbook of Infrared and Raman Characteristic Frequencies of Organic Molecules*. Academic Press, Boston, 1991
30. K.L. Johnson, *Contact Mechanics*. Cambridge University Press, Cambridge, 1985
31. X. Li, Y.H. An, Y.D. Wu, Y.C. Song, Y.J. Chao, and C.H. Chien, Microindentation Test for Assessing the Mechanical Properties of Cartilaginous Tissues, *J. Biomed. Mater. Res. B Appl. Biomater.*, 2006, p 25–31
32. Y.Y. Lim and M.M. Chaudhri, Indentation of Elastic Solids with a Rigid Vickers Pyramidal Indenter, *Mech. Mater.*, 2006, **38**, p 1213–1228